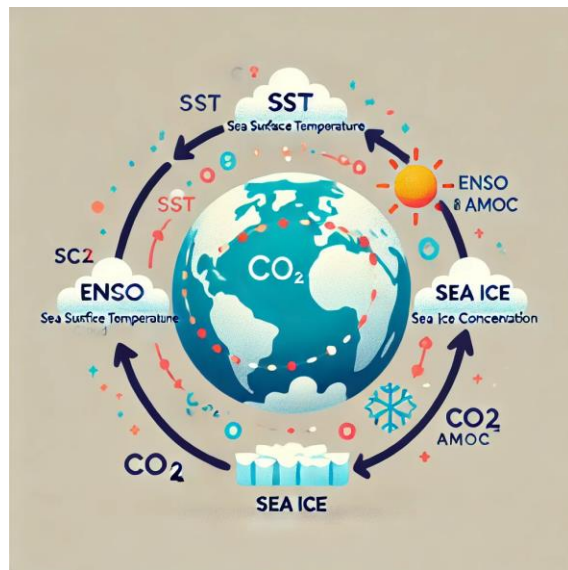


Scientific report

“Searching for anthropogenic and natural footprints in observed global cloud and sea ice cover fields, through a synergetic approach” (CLIMATICFOOTPRINTS)

Dr. Petru Cosmin Vaideanu

Prof. Dr. Mihai Dima



I. Background and Motivation

Global climate change represents one of the most pressing scientific and socio-political challenge of the 21st century. Of particular importance is the need to accurately distinguish between natural climate variability and anthropogenic (human-induced) influences, which is essential for improving the accuracy of future projections made with climate models and for guiding climate policies. This project was implemented to address this critical scientific need by focusing on two key components of the climate system: global cloud cover and sea ice concentration. Scientific research was performed through advanced statistical analyses of state-of-the-art climate modeling, reanalysis, and observational data in order to separate the naturally and anthropogenically-induced impact on these two components.

II. Goals

The main goal of this research project was to provide a distinction of the anthropogenic and natural induced impact on observed fields/variables of two of the most sensitive climate components: clouds and sea ice. A second goal was to provide an observational reference framework which can be used as a comparison for model simulations of global cloud and sea ice cover, in terms of structure, temporal evolutions, and quantified contributions of important forcing factors.

Over the course of the project, both the primary and the secondary objectives were achieved through the following steps, in accordance with the research proposal:

- Diagnosis of the observed, reanalysis and model total cloud and sea ice cover data (stage 1)
- Identification of anthropogenic and natural footprints in observed total cloud cover and sea ice concentration data (stage 2)
- Identification of anthropogenic and natural footprints in reanalysis total cloud cover and sea ice concentration data (stage 2)
- Identification of anthropogenic and natural footprints in AWI-ESM2.1 climate model total cloud cover and sea ice concentration data (stage 3)
- Extensive comparison and synthesis of the results (stage 3)

III. Dissemination of results

A key indicator of success in disseminating results was the publication of scientific papers in high-impact journals. To date, two papers have been published, one is in the second review phase and two are under open review (see below). This surpasses the initial dissemination plan, which included 3 scientific papers:

- **Scientific paper (published):** *Large-scale sea ice–surface temperature variability linked to Atlantic meridional overturning circulation, Journal:* PLOS ONE (5yr Impact Factor: ~3.5).

Authors: Petru Vaideanu, Christian Stepanek, Mihai Dima, Jule Schrepfer, Fernanda Matos, Monica Ionita, Gerrit Lohmann

<https://journals.plos.org/plosone/article?id=10.1371/journal.pone.0290437>

- **Scientific paper (published):** *Deconstructing Global Observed and Reanalysis Total Cloud Cover Fields Based on Pacific Climate Modes*, **Journal:** Atmosphere (5yr Impact Factor: ~2.7). **Authors:** Petru Vaideanu, Monica Ionita, Mirela Voiculescu and Norel Rimbu
<https://www.mdpi.com/2073-4433/14/3/456>
- **Scientific paper (review-accepted for publication):** *Examining the Eastern European heatwave of 2023 from a long-term perspective: the role of natural variability vs. anthropogenic factors*. **Journal:** Natural Hazards and Earth System Sciences (5yr Impact Factor: ~4.2). **Authors:** Monica Ionita, Petru Vaideanu, Bogdan Antonescu, Catalin Roibu, Qiyun Ma, and Viorica Nagavciuc
<https://egusphere.copernicus.org/preprints/2024/egusphere-2024-1207>
- **Scientific paper (late review):** *Interplay of Anthropogenic and Natural Drivers of Observed Coupled Sea Surface Temperature - Arctic Sea Ice Variability*, **Journal:** Climate Dynamics (5yr Impact Factor: ~4.4). **Authors:** Petru Vaideanu, Mihai Dima, Denis Nichita, Cristian Stepanek, Paul Gierz, Norel Rimbu, Monica Ionita and Gerrit Lohmann
- **Scientific paper (open review)** *Trends and Variability of Heat Waves in Europe and the Association with Large-Scale Circulation Patterns*. **Journal:** (Social Science Research Network (5yr Impact Factor: ~2.2). **Authors:** Loredana Boboc, Mihai Dima, Petru Vaideanu, Monica Ionita
https://papers.ssrn.com/sol3/papers.cfm?abstract_id=4941618

**For the manuscripts currently under review, in the revised and final published version of the manuscript, the following text will be included in the funding section, acknowledging this project: P.V. was funded by project PN-III-P1-1.1-PD-2021-0505, Ctr:28/2022, CLIMATICFOOTPRINTS of the Romanian UEFISCDI.*

The most important result: The project provided new insights into how internal climate modes, such as El-Nino Southern Oscillation (ENSO) and Atlantic Meridional Overturning Circulation (AMOC), influence global cloud and sea ice variability and their weight in comparison with anthropogenic influence.

In addition, during my three-month research stay at the Alfred Wegener Institute for Polar and Marine Research in the Paleoclimate Dynamics group (June-August 2023, 2024), financed by the HIDA Research Visiting Grant (<https://www.helmholtz-hida.de/en/new-horizons/hida-visiting-program/>), I focused on gathering and started analyzing SST-SIC data from the AWI-ESM2.1 climate model. My time at AWI marks a significant stepstone in the collaboration between AWI and University of Bucharest to and was key part for successfully completing the last phase of the project.

A small deviation from the initial plan was related to a change in conference attendance. Due to uncertainties in the visa process for the USA, participation in the AGU 2023 conference was replaced with participation at the German Environmental Award and two national conferences.

- *European Geoscience Union (EGU 2024) – poster presentation*
- *German Environmental Award (Deutscher Umweltpreis), October 2023, Lubeck, Germany*
- *Modern Approaches of the Environment-Climate Change Interconnectivity, September 2023, Galati, Romania.*

- *Global Solutions Summit 2023*, May 2023, Berlin, Germany.
- *Symposium* at Deutsche Bundesstiftung Umwelt (DBU) Alumni Meeting, March 2023, Cluj Napoca, Romania.

The project was conducted as planned in the initial proposal and all the anticipated risk were overcome due to the excellent collaboration between the project leader, the mentor and colleagues from the University of Bucharest, the University “Dunarea de Jos” Galati and the Alfred Wegener Institute for Polar and Marine Research (AWI). Only minor discrepancies can be observed in expected versus achieved results, primarily due to the inherent complexities of climate system dynamics and data limitations.

IV. Project’s impact

The project has had a significant impact on the scientific community by contributing to the growing understanding of natural and anthropogenic influences on cloud and sea ice recent variability, two of the most important components of the Earth's radiative balance.

Key contributions:

- *Understanding large scale climate variability*: The project provided new insights into how internal climate modes, such as ENSO and AMOC, influence global cloud cover and sea ice concentration variability and their weight in comparison with anthropogenic influence.
- *Reduction of Uncertainty in Climate Models*: The identification of anthropogenic footprints in global cloud cover and Arctic sea ice has helped reduce uncertainty in climate models, regarding future projections. It is argued that “*a correct representation of AMOC-induced coupled SST–SIC variability in climate models is essential to understand the past, present and future sea-ice evolution*” (Vaideanu et al 2023b).
- *Collaborations with Leading Research Institutes*: The research stays at the Alfred Wegener Institute for Polar and Marine Research (AWI) in Germany provided access to advanced modeling tools and high-quality datasets. This collaboration significantly contributed to the project leader’s ability to analyze sea ice variability and interactions with oceanic processes. The exchange of ideas with researchers at AWI also facilitated valuable knowledge transfer and collaboration opportunities for future projects.
- *Public Awareness*: Policymakers can use the project’s findings to support strategies that address both mitigation and adaptation to climate change. In particular, the findings related to Arctic sea-ice decline, driven by human activities (Vaideanu et al., 2024, under review), underscore the need for urgent action in polar conservation efforts.

V. Project overview and results

The project was conducted at the Faculty of Physics, University of Bucharest under the mentorship of Prof. Mihai Dima. The research was structured in multiple stages:

- *Stage 1: Data Diagnosis and Preparation*

This phase focused on diagnosing and preparing the data to be used throughout the project. Total cloud cover (TCC) and sea-ice concentration (SIC) data were collected from a variety of sources, including observational fields obtained from direct measurements, reanalysis datasets generated by assimilating observational data into general circulation models (GCMs), and outputs from numerical simulations performed using AWI-ESM2.1

- *Stage 2: Data Analysis and Identification of Coupled Interactions*

Building upon the groundwork laid in Stage 1, the second phase focused on the complex statistical analysis of the data. During this phase, Canonical Correlation Analysis (CCA) was extensively used to explore interactions between sea surface temperature (SST), total cloud cover, and sea-ice concentration.

- *Stage 3: Analysis Using the AWI-ESM2.1 Climate Model*

The final phase of the project utilized the Alfred Wegener Institute Earth System Model (AWI-ESM2.1), a state-of-the-art coupled climate model, to analyze simulated cloud cover and sea-ice data under different atmospheric CO₂ scenarios.

Stage 1

1.1 Data selection

In a preliminary stage, for all datasets used, monthly anomalies from the annual cycle are calculated relative to 1980 – 2010 period and then annual means are computed. In order to isolate possible footprints of climate-internal modes of variability cloud and sea-ice data derived from reconstructions, reanalyzes and model simulations is filtered by applying linear detrending. The removal of the trends increases the signal-to-noise ratio in the data and facilitates identification of modes of internal variability.

Table 1**Main characteristics of the used data processed**

Data	Type	Period	Resolution	Variable
NSIDC	Observations	1979 - present	1° x 1°	Sea ice cover
HadISST	Observations	1980 - present	1° x 1°	Sea ice cover
ISCCP	Observations	1984 - 2009	5° x 5°	Total cloud cover
PATMOSx	Observations	1984 - 2009	2.5° x 2.5°	Total cloud cover
GPCP V2.2	Observations	1979 - present	2.5° x 2.5°	Total precipitation rate
HadISST	Observations	1870 - present	1° x 1°	Sea surface temperature
ERSSTv3.b	Observations	1854 - present	2° x 2°	Sea surface temperature
ERA-Interim	Reanalysis	1979 - present	3° x 3°	All of the above
ERA 20C	Reanalysis	1900 - 2010	3° x 3°	All of the above
NCEP/NCAR	Reanalysis	1948 – present	2.5° x 2.5°	All of the above
20 th Century Re.	Reanalysis	1854 - 2015	2.5° x 2.5°	All of the above
AWI-ESM2.1	Global climate model	1850 - 2100	1° x 1°	Sea surface temperature
AWI-ESM2.1	Global climate model	1850 - 2100	1° x 1°	Sea level pressure
AWI-ESM2.1	Global climate model	1850 - 2100	1° x 1°	Sea ice cover
AWI-ESM2.1	Global climate model	1850 - 2100	1° x 1°	2m Surface Temperature

1.2 Data diagnosis using Empirical Orthogonal Functions (EOF) method

The Empirical Orthogonal Function (EOF, Lorenz 1951) is a statistical method that uses an orthogonal transformation to transform a set of observations of correlated variables into a set of values of non-correlated linear variables. The uncorrelated variables represent linear combinations of the initial ones. The first main component explains the maximum amount of the variance from the original variables; the second one explains the maximum amount of the remaining variance, not explained by the first component, and so on. It is the simplest multivariate analysis method based on eigenvectors and reveals the internal structure of the data in a way that best explains their variability in the spatial domain (Levine and Wilks, 2000). In other words, the EOF allows us to reduce the size of the data for a compact and optimal description of them, thus increasing the signal to noise ratio, in many cases.

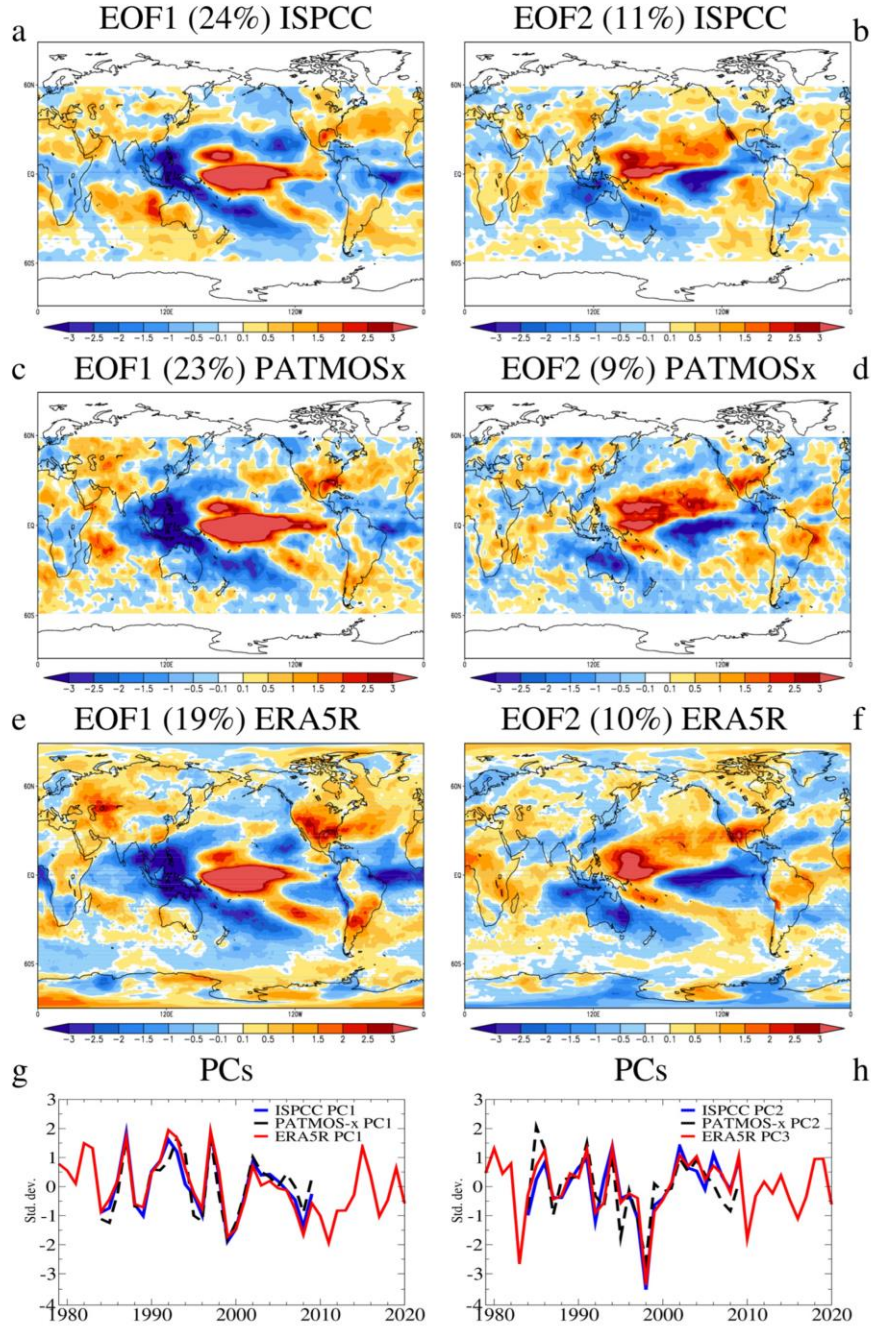
1.3 Comparison of the dominant modes of variability identified through the EOF method

The first two modes of total cloud cover (TCC) variability, derived through the EOF analysis on the annual cloud anomalies from ISCCP and PATMOS-x and ERA5 datasets, are shown in Figure R1. The spatial structures of EOF1 show both qualitative and quantitative similarities across much of the globe. The highest loadings appear in the tropical Pacific, marked by a band of positive TCC anomalies stretching from the west coast of Peru to the Central Pacific, with negative loadings in the Central, Northeast, and Southeast

Pacific. Positive anomalies are also present over North America, Central Asia, and the North Atlantic, being more pronounced in ERA5 and less intense in PATMOS-x. Negative values extend over the tropical Atlantic, reaching northeastern South America. Differences between observed and reanalyzed EOF1 patterns are noticeable over regions like Australia, northwestern South America, and the South Atlantic (Vaideanu et al. 2023a). The corresponding time series (PC1) are dominated by interannual variability and are strongly correlated ($r = 0.89$, significant at the 99% level).

The spatial structures of the second EOF, derived from ISCCP, PATMOS-x, and ERA5 are characterized by an equatorial dipole of TCC anomalies in the equatorial Pacific, with intense positive loadings in the central region and negative anomalies in the east. Additionally, there is an increase in cloud cover over northeastern South America extending to the tropical Atlantic and a decrease in cloudiness over the North Atlantic. The associated principal components (PCs) show no clear trend and have a correlation coefficient of 0.77 (significant at the 99% level). Both EOFs feature their maximum positive TCC anomalies in the tropical Pacific, with their PCs driven by interannual variability. The combined variance explained by the first two modes is 35% for ISCCP and 32% for PATMOS-x, while about 55% of the remaining variance is distributed almost equally among numerous modes, each explaining less than 5%, likely associated with noise (Vaideanu et al. 2023a).

Figure R1. Global modes of TCC variability (Vaideanu et al. 2023, Source: <https://www.mdpi.com/2073-4433/14/3/456>) *Left column: The spatial structure of the dominant mode (EOF1) of TCC variability (%) based on ISCCP (a), PATMOS-x (c) and ERA5 reanalysis (e) data with their associated time series (g). Right column: The second empirical orthogonal function (EOF2) of TCC variability (%) based on ISCCP (b) and PATMOS-x (d) data and the third EOF from ERA5 reanalysis (f) data, with their associated time series (h).*



Similarly, the leading mode of SIC variability (EOF1) derived from observed NSIDC SIC annual anomalies for the period 1950–2017 is presented in Figure R2. This mode accounts for approximately 34% of the total variance, with the most notable negative anomalies concentrated over the East Greenland, Barents, and Kara Seas, and less prominent over Baffin Bay. The corresponding time series (Figure R2b) reveals a significant increasing trend, which becomes particularly pronounced after the 1980s (Vaideanu et al. 2023b). The increasing trend in the associated time series reflects intense ongoing changes in Arctic sea ice, especially post-1980s, which aligns with broader patterns of Arctic climate change.

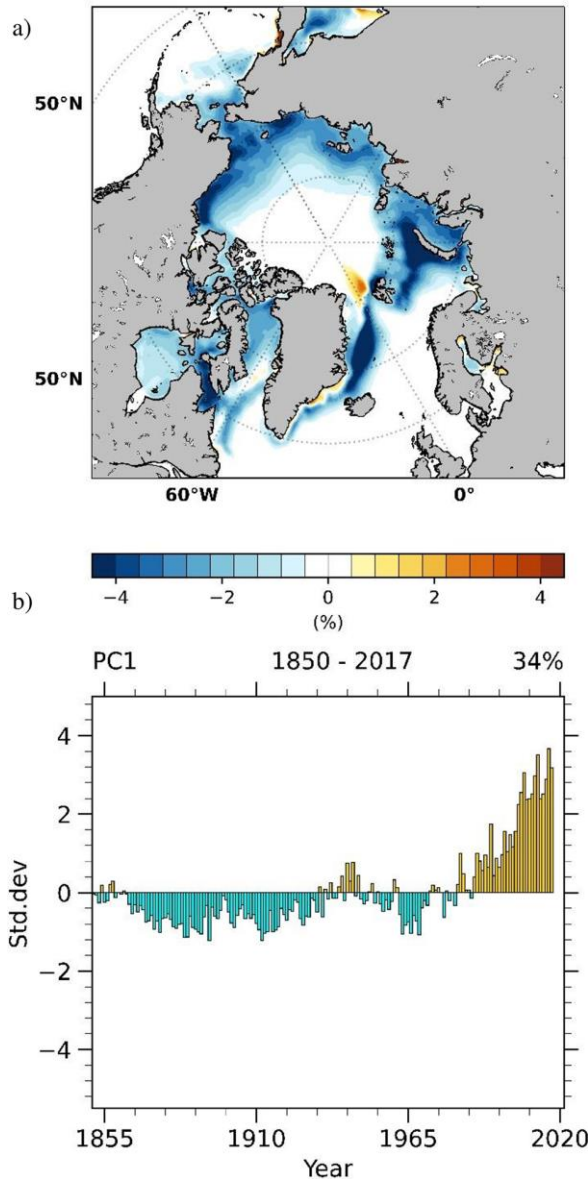


Figure R2. Dominant mode of observed sea-ice concentration (SIC) variability identified from annual NSIDC SIC anomalies (Vaideanu et al. 2023b). The pattern of the dominant mode (EOF1) of Arctic SIC variability (a), explaining 34% of variance, together with its associated time series (b). Source <https://doi.org/10.1371/journal.pone.0290437.g001>

In Stage 1, key data gathering, and methodologies were successfully implemented. Preliminary analyses were performed, setting the stage for more detailed investigations. The results from EOF analysis provide valuable insights into the complex interactions influencing cloud and sea ice variability on a global scale.

Stage 2

Building upon the Empirical Orthogonal Functions (EOFs) analysis conducted in Stage 1, which identified key spatial patterns in climate data, Stage 2 involved numerous Canonical Correlation Analysis (CCA) between Total Cloud Cover (TCC) and Sea Ice Concentration (SIC) with Sea Surface Temperature (SST) fields, using both observational and reanalysis data. CCA is a powerful multivariate technique used to identify pairs of patterns with maximum correlation between their associated time series. As the core constraint of the method is the maximization of correlation between time components, the corresponding patterns are identified by the method even if they do not explain a large amount of the variance in their fields (Levine and Wilks 2000). Mathematically, CCA transforms pairs of originally centered vectors X_0 and Y_0 into sets of new variables, called canonical variables. CCA is a useful tool to identify the footprint of a forcing factor on a given field when distinct forcing factors are characterized by different temporal evolutions because it is based on the distinction between time evolution of patterns. In order to increase this ratio and therefore to maximizes the CCA effectiveness each of the two initial fields (e.g., SST and SIC) is decomposed in a linear combination of EOFs and then is reconstructed back based only on the first twelve modes (Levine and Wilks 2000).

2.1 Canonical Correlation Analysis (CCA) between Total Cloud Cover (TCC) and Sea Ice Concentration (SIC) with Sea Surface Temperature (SST) fields, using observational and data

Coupled CCA pairs of observed SST-TCC variability revealed the main drives behind the variability of the dominant TCC modes identified in Stage 1. The SST spatial structure of the third pair (Figure R3a) explains 20% of the total variance, dominated by positive anomalies in the eastern tropical Pacific, surrounded by negative values, reflecting the typical Eastern Pacific (EP) ENSO pattern. Its corresponding TCC structure (Figure R3e) shows positive anomalies in the eastern-central Pacific and over the North and South Atlantic, with negative anomalies in the western-central Pacific and parts of the northeast and southeast Pacific. This TCC structure explains 22% of the total cloud cover variance and strongly projects onto EOF1 (projection coefficient = 0.94). The associated time series (Figure R3c) is characterized by inter-annual variability, significantly correlated with the Niño3 Index ($r = 0.84$). The SST spatial structure of the fourth pair (Figure R3b), features positive values in the central tropical Pacific, forming a V-shaped anomaly extending toward the subtropics, and negative anomalies near the northwest coast of South America, characteristic of Central Pacific (CP) ENSO events. The associated TCC structure (Figure R3f) has high loadings in the Central Pacific, with positive anomalies in the central tropical region and negative anomalies in the eastern Pacific. The time series of this pair is significantly correlated ($r = 0.67$) with the Trans-Niño Index (TNI), further linking it to CP ENSO events (Vaideanu et al. 2023a).

A similar CCA was performed using the PATMOS-x total cloud cover data (Figure R4).

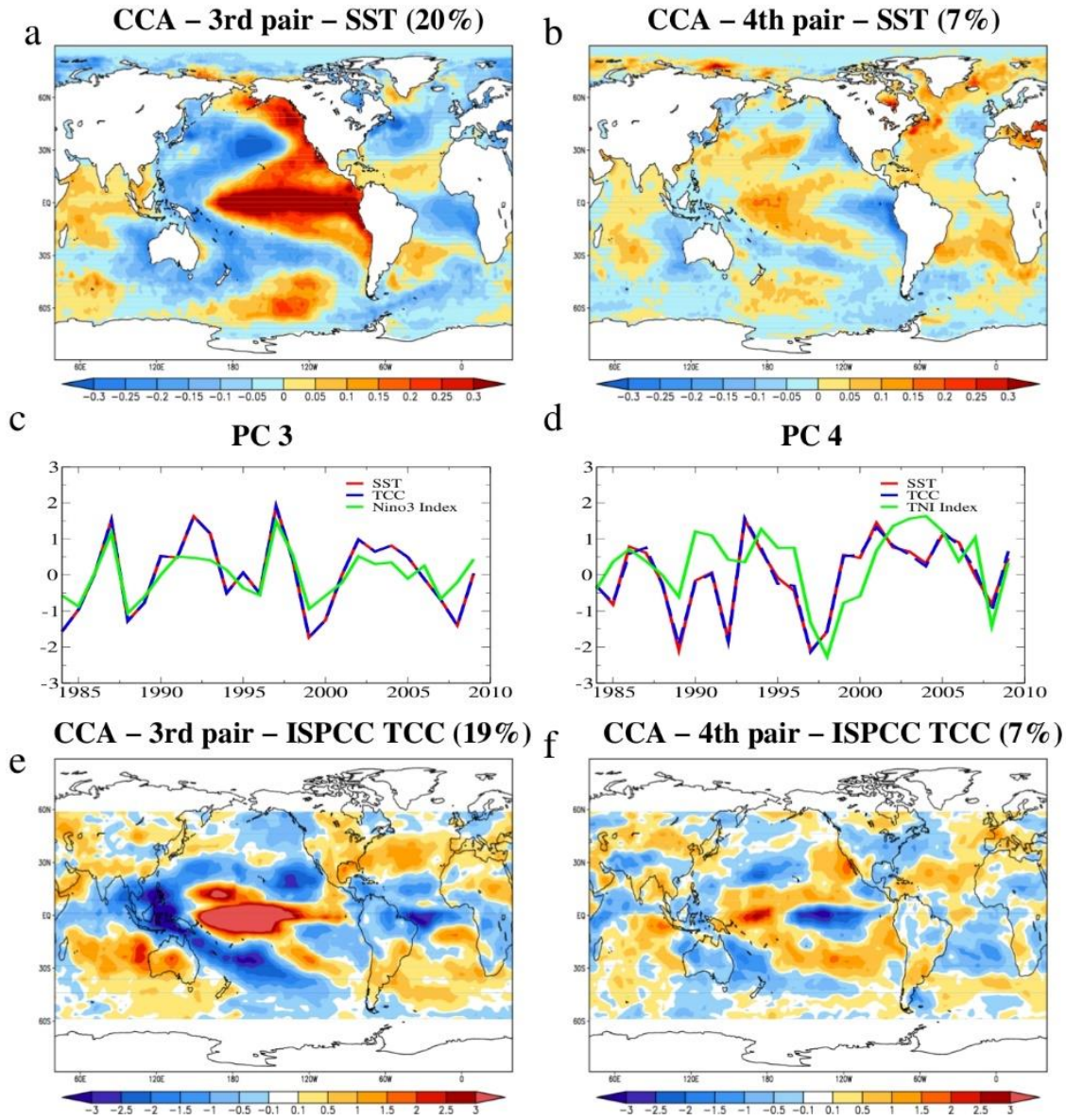


Figure R3. The EP ENSO (left) and the CP ENSO (right) footprints on global SST-TCC fields identified through CCA using ISPCC observations of total cloud cover data extending over 1984 – 2009 period (Vaideanu et al. 2023a, Source: <https://www.mdpi.com/2073-4433/14/3/456>). Left column: The third coupled SST ($^{\circ}\text{C}$) - TCC (%) pair: the SST pattern (a), explaining 20% of variance, the TCC structure (e), explaining 19% and the associated time series (c) with TCC (blue line), SST (red line). The correlation with the Niño3 Index (green line) is 0.81. Right column: The forth coupled SST ($^{\circ}\text{C}$) - TCC (%) pair: the TCC pattern (a), explaining 7% of variance, the SST structure (c), explaining 7% and the associated time series (e) with TCC (blue line), SST (red line). The correlation with the TNI Index (green line) is 0.61.

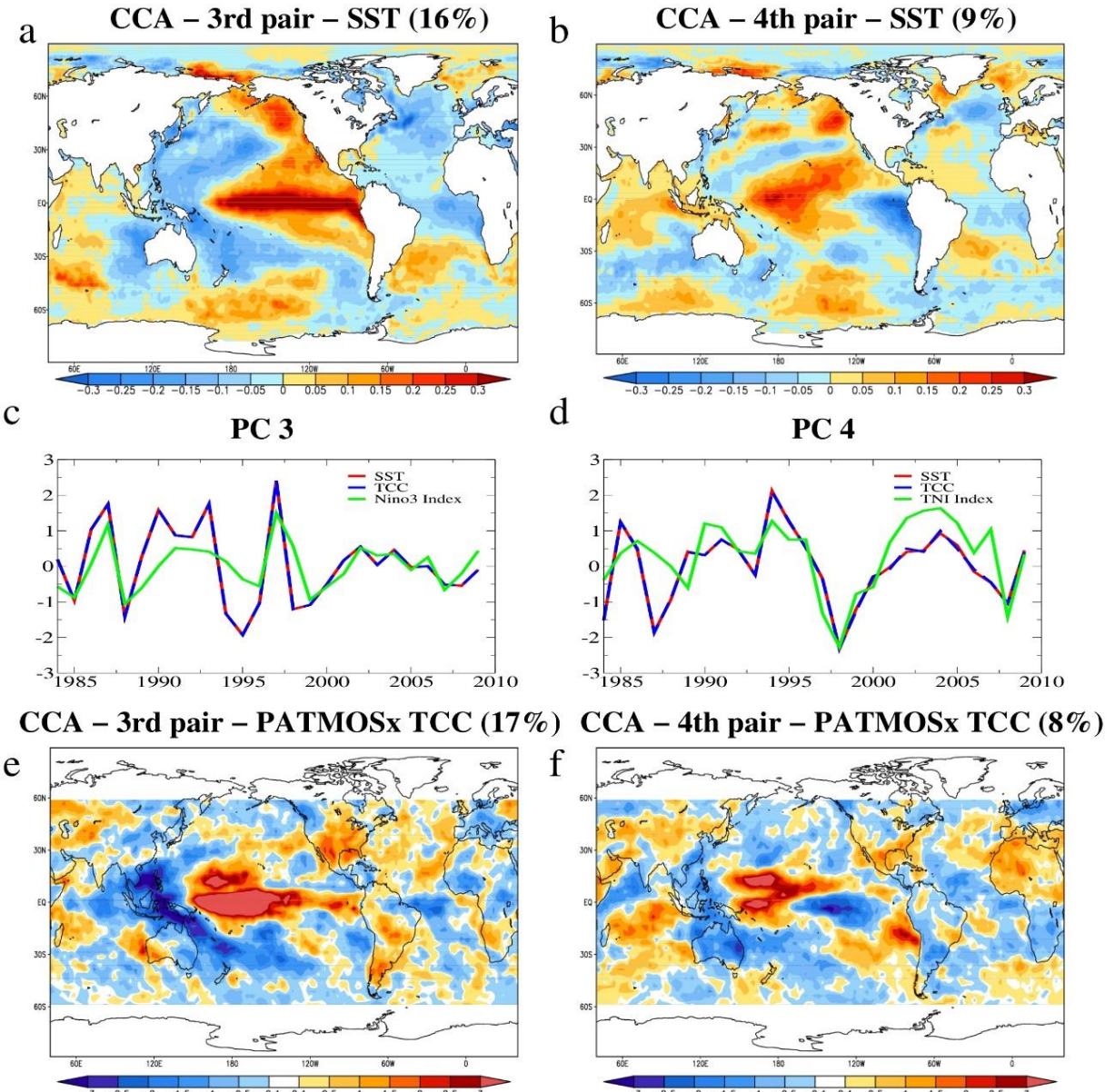


Figure R4. The EP ENSO (left) and the CP ENSO (right) footprints on global SST-TCC fields identified through CCA using PATMOS-x observations of total cloud cover data extending over 1984 – 2009 period. (Vaideanu et al. 2023a, Source: <https://www.mdpi.com/2073-4433/14/3/456>). Left column: The third most coupled SST ($^{\circ}\text{C}$) - TCC (%) pair: the SST pattern (a), explaining 16% of variance, the TCC structure (e), explaining 17% and the associated time series (c) with TCC (blue line), SST (red line). The correlation with the Niño3 Index (green line) is 0.79. Right column: The fourth most coupled SST ($^{\circ}\text{C}$) - TCC (%) pair: the TCC pattern (b), explaining 9% of variance, the SST structure (f), explaining 8% and the associated time series (d) with TCC (blue line), SST (red line). The correlation with the TNI Index (green line) is 0.73.

The pairs from Figure R3 and R4 show that global interactions between SST and TCC are influenced predominantly by the Eastern Pacific (EP) and Central Pacific El Niño—Southern Oscillation (CP ENSO)

modes (internal variability). The analyses highlighted the significant role of these ENSO modes in driving global coupled SST–TCC variability, with the Central Pacific ENSO explaining a substantial portion of this variance. These results emphasize the crucial influence of Pacific modes of internal variability on global cloud dynamics (Vaidneau et al. 2023a).

Anthropogenic influence on Total Cloud Cover variability

To identify the impact of the main anthropogenic forcing (IPCC 2021) on the SST and TCC fields, these have been regressed on the atmospheric CO₂ concentration index provided by the Mauna Loa Observatory (Figure R5). The regression maps of both SST data are dominated by positive anomalies extending over almost all the globe (Figure R5a and b), with maximum values in the Indian Ocean and minimum loadings in the Southern Ocean, consistent with the greenhouse effect induced by the atmospheric CO₂. Both TCC maps (Figure R5c and d), are dominated by negative loadings at mid-latitudes, more prominent in the one obtained using ISPCC data. Similar global patterns of TCC variability have been associated with the climate change impact on TCC in a study based on observational data and numerical simulations (Norris et al. 2016). They also found the impact of this greenhouse gas on most of the regions around 40° N and 40° S to be statistically significant.

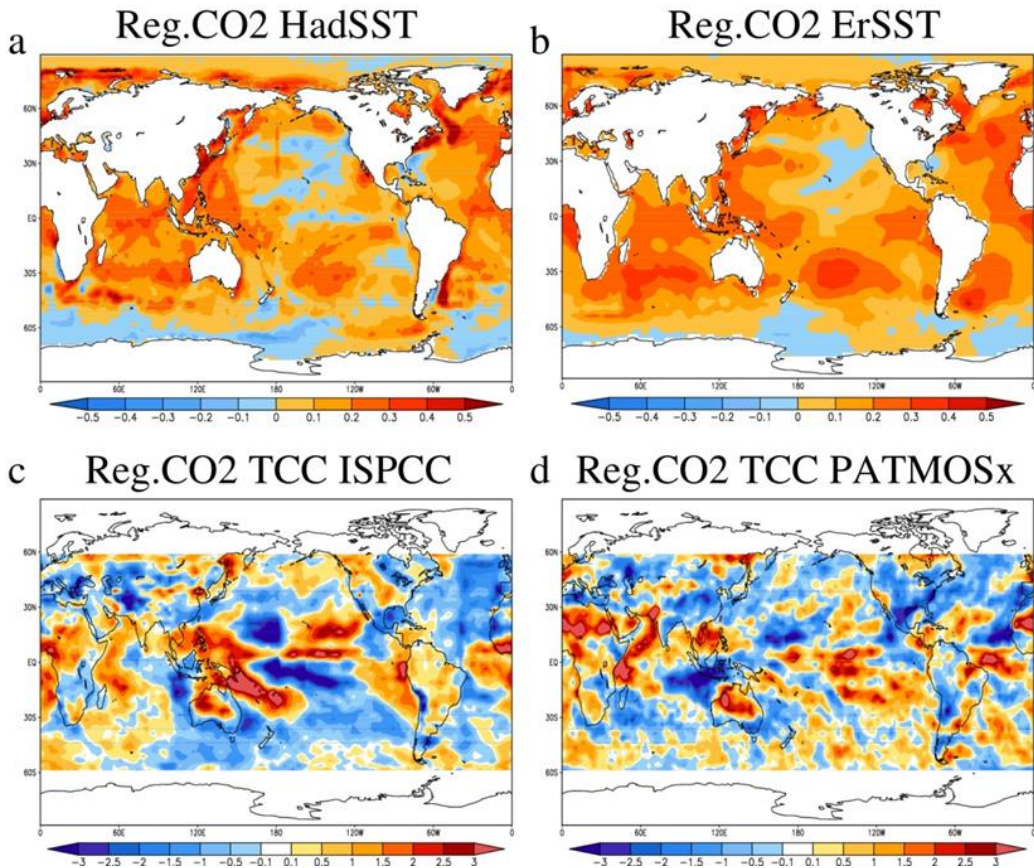


Figure R5. Anthropogenic footprint on global SST (top) and TCC (bottom) fields .Regression maps of HadISST (a), ErSST (b), ISPCC (c), and PATMOS-x (d) on the time series of the CO₂ concentration Index from Mauna Loa Observatory extending over 1984 – 2009 for cloud data and 1950 – 2022 for SST data

Anthropogenic, oceanic, and atmospheric drivers of observed coupled sea surface temperature - sea ice variability

In order to identify the footprints of various potential causes on the sea ice field, multiple CCAs were performed between the corresponding SST and SIC fields with results shown in Figure R6. The spatial pattern of the first CCA pair shows quasi-uniform positive anomalies, particularly strong in the Indian Ocean, reflecting the classic SST response to climate change (Figure R6a). The associated SIC pattern (Figure R6c) is characterized by negative anomalies across the Arctic, especially in the Greenland, Barents, Kara, and Laptev seas. The time series for both SST and SIC patterns display a significant upward trend, indicating a strong link to increasing atmospheric CO₂ levels and their greenhouse effect. These findings align with previous studies, which attribute the decline in Arctic sea ice and the overall warming of SSTs globally to anthropogenic climate change driven by rising CO₂ concentrations (Vaideanu et al., 2024, under review).

The second CCA pair, explaining 9% of Arctic SIC variance, is linked to the positive phase of the Atlantic Multidecadal Oscillation (AMO), based on the SST structure (Figure R6d), which shows positive loadings over the North Atlantic and negative anomalies over the southern Atlantic. The SIC pattern (Figure R6f) shows negative anomalies over much of the Arctic and Baffin Bay, and particularly strong loadings in the Barents and Kara seas, attributed to changes in heat transport driven by the AMO (Vaideanu et al., 2024, under review). The time series of SST and SIC patterns of this pair are significantly correlated with the AMO Index.

The third CCA pair reflects the influence of the North Atlantic Oscillation (NAO) on SST (Figure R6g) and SIC (Figure R6i) fields. The SST field shows a tripolar-like structure, with positive loadings in the North Atlantic and negative loadings over the subpolar gyre, a pattern driven by the NAO's negative phase. The associated SIC pattern features negative anomalies over the Barents Sea and positive anomalies in Baffin Bay and the Beaufort Sea. The NAO affects SIC through surface temperature changes and wind-driven sea ice advection. Over the Barents Sea, the NAO's influence on sea ice decline is linked to both surface temperature and wind patterns, while over Baffin Bay, cold Arctic air driven by the NAO increases sea ice accumulation (Vaideanu et al., 2024, under review).

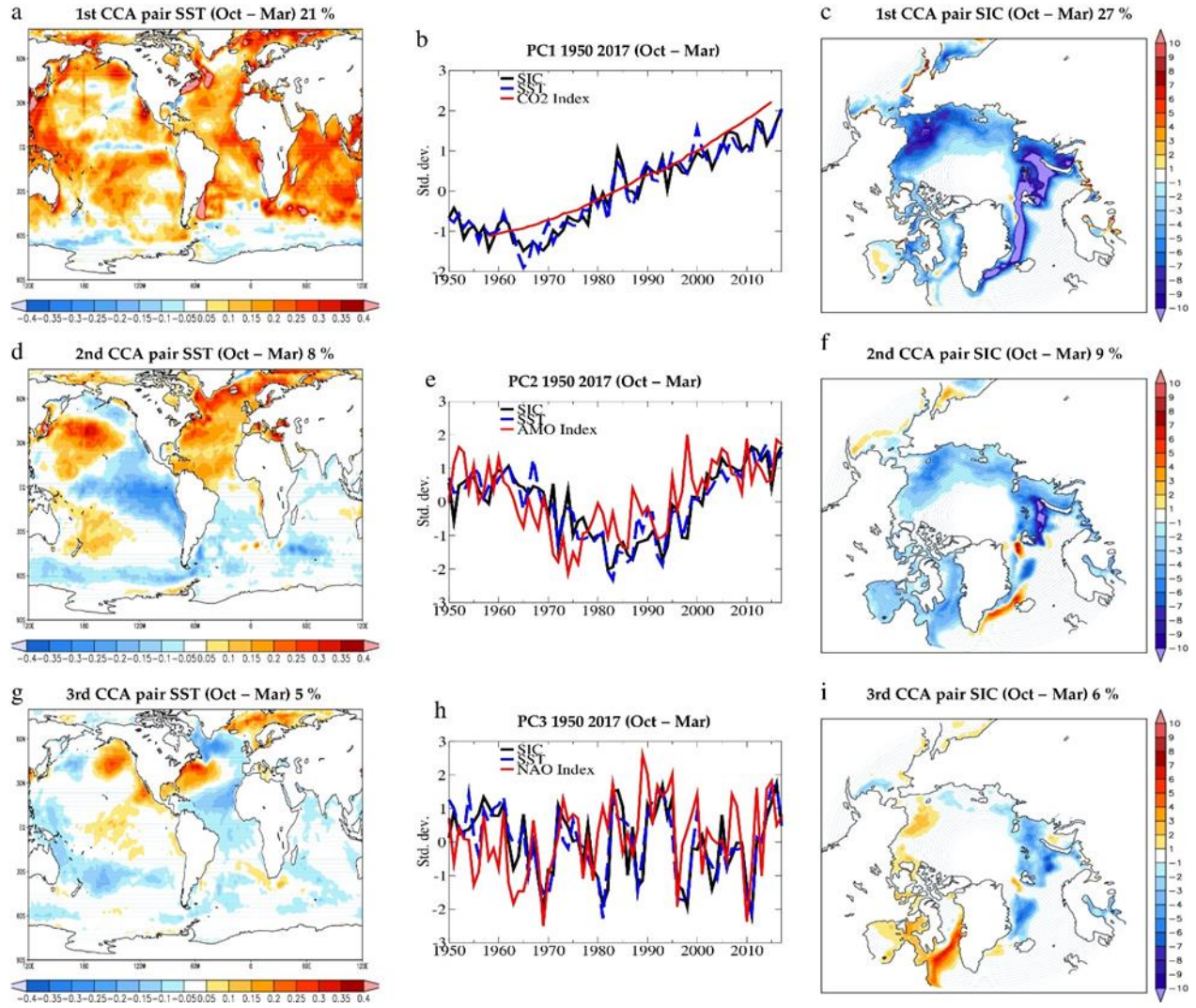


Figure R6. Coupled SST-SIC patterns identified through CCA between the corresponding October – March HadISST ($^{\circ}\text{C}$) and NSIDC Reconstruction.V2 SIC (%) fields over the 1950-2017 period

Top row: The first coupled CCA pair derived through CCA: the SST pattern (a) explaining 21% of variance and the SIC structure (c), explaining 27% of variance. Their temporal evolution (b) has a correlation coefficient of 0.99. *Second row:* The second coupled CCA pair: The SST pattern (d) explaining 8% of variance and the SIC structure (f), explaining 9% of variance. Their temporal evolution (e) has a correlation coefficient of 0.98. Their correlation with the AMO index (e, red line) is 0.71. *Third row:* The third coupled CCA pair: the SST pattern (g) explaining 5% of variance and the SIC structure (h), explaining 6% of variance. Their temporal evolution (i) has a correlation coefficient of 0.965. Their correlation with the NAO index (h, red line) is 0.79

2.2 Canonical Correlation Analysis (CCA) between Total Cloud Cover (TCC) and Sea Ice Concentration (SIC) with Sea Surface Temperature (SST) fields, using reanalysis data

To assess coupled Atlantic SST and global SIC variability from 1959 to 2021, a CCA was performed using annual detrended SST anomalies from ErSSTv5 and SIC anomalies from the ERA5 Reanalysis (Vaideanu

et al., 2023b). The first CCA pair's SST structure (Figure R7a) displays opposite North-South Atlantic anomalies, reflecting the Atlantic Meridional Overturning Circulation (AMOC's) multi-decadal SST pattern. Over Antarctica, the SIC pattern (Figure R7d) shows positive loadings around the Peninsula extending toward the Weddell and Bellingshausen Seas, with negative values toward the Pacific Ocean. The time series evolution shows no significant trend over the period 1959–2021. The bipolar SST-SIC structure, where warm SSTs in the Northern Hemisphere correlate with Arctic sea ice loss and cool SSTs in the Southern Hemisphere with increased Antarctic sea ice, suggests that AMOC variations partly drive Antarctic sea-ice changes during this period (Vaideanu et al. 2023b). However, other factors, such as Rossby waves, the Antarctic Oscillation, and ozone layer composition, also contribute to Antarctic SIC variability.

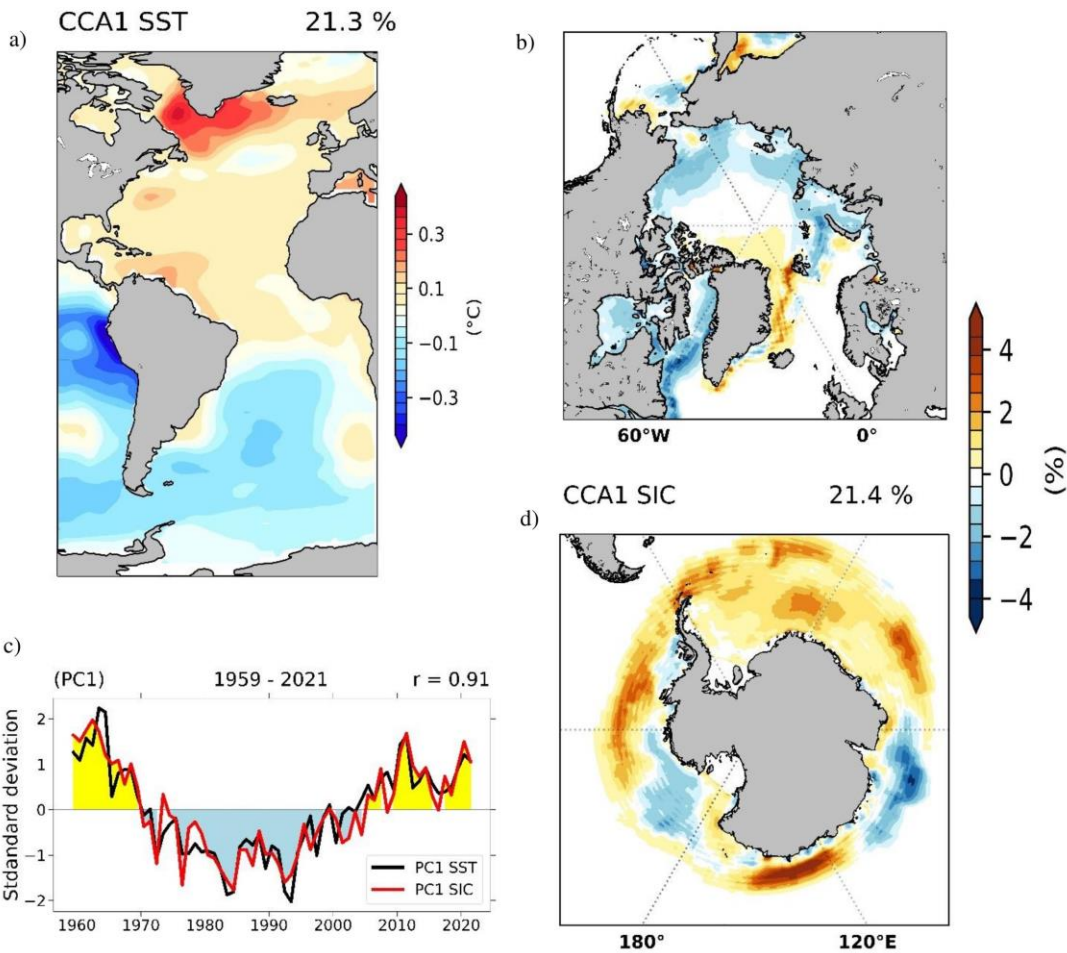


Figure R7. AMOC footprint on Atlantic SST – Global SIC, identified through CCA between the corresponding ErSSTv5 and ERA5 Reanalysis annual detrended anomalies extending over the 1959 - 2021 period (Vaideanu et al. 2023b, Source:

<https://journals.plos.org/plosone/article?id=10.1371/journal.pone.0290437>). Left column: The third most coupled TCC SST (°C) - TCC (%) pair identified through CCA using ERA5 TCC data: the TCC

pattern (a), explaining 16% of variance, the SST structure (c), explaining 13% and the associated time series (e) with TCC (blue line), SST (red line). The correlation with the Niño3 Index (green line) is 0.89. *Right column:* The fifth most coupled SST (°C) - TCC (%) pair: the TCC pattern (b), explaining 7% of variance, the SST structure (f), explaining 7% and the associated time series (d) with TCC (blue line), SST (red line). The correlation with the TNI Index (green line) is 0.71

2.3 Identifying the physical mechanisms associated with the coupled SST – TCC and SST - SIC links identified through CCA

To substantiate the relationship between the identified first coupled Atlantic SST-Arctic SIC pair and AMOC presented above, we conducted a correlation analysis using global Surface Air Temperature (SAT) and Total precipitation Rate (TPR) fields from the NCEP/NCAR 20th Century Reanalysis with the time components of this CCA pair. The resulting correlation maps (Figure R8a) reveal a significant positive correlation over key Arctic regions like Greenland, Kara, and Barents Seas, indicative of the influence of AMOC on northward heat transport. In contrast, the Antarctic (Figure R8a) displays a significant anti-correlation, illustrating the inter-hemispheric temperature dichotomy associated with AMOC-induced variations in the global energy distribution (Jackson et al. 2015). This pattern suggests an AMOC impact on the Atlantic's temperature gradients, consequently affecting the Intertropical Convergence Zone's position, as also supported by the TPR correlation map showing a northward ITCZ shift in the Atlantic (not shown).

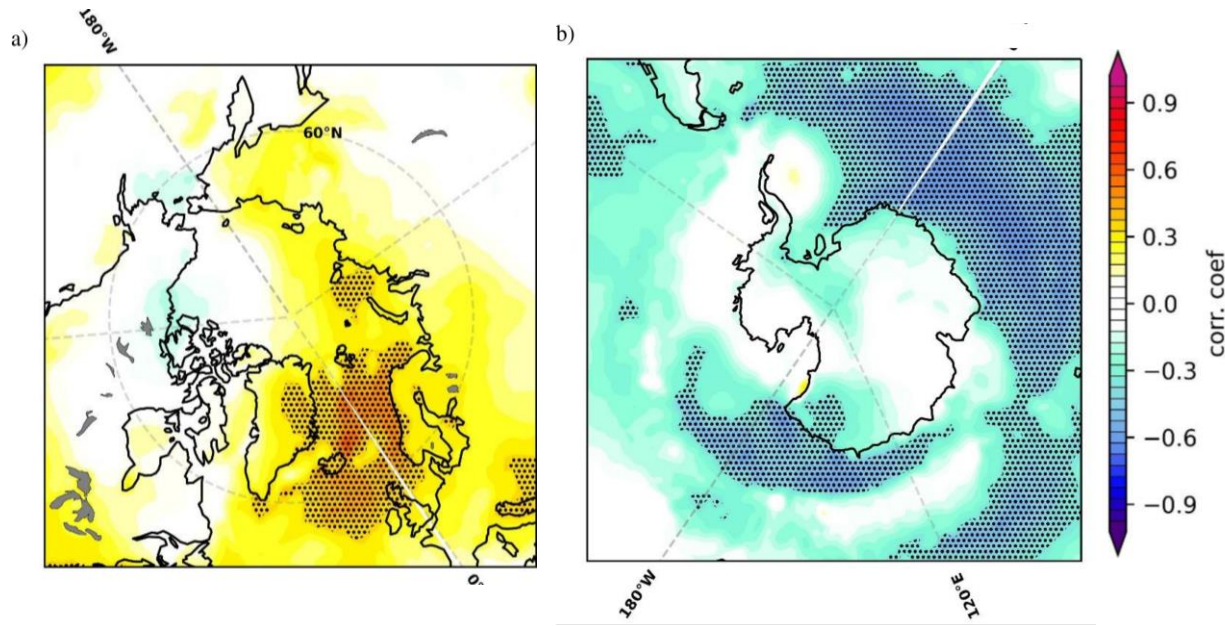


Figure R8 | Inter-hemispheric temperature dipole. Correlation map between global detrended annual anomalies from the 20th Century Reanalysis surface air temperature (SAT) and the time series of the observed CCA pair that is investigated in relation to AMOC (Fig 2c), plotted from 55°N – 90°N (a) and from 50°S – 90°S (b), over the 1854-2015 period. The associated statistical significance in hatched areas exceeds 95 %. (Vaideanu et al. 2023b, Source: <https://journals.plos.org/plosone/article?id=10.1371/journal.pone.0290437>)

2.4 Comparison and synthesis of the results

Comparative insights of observational and reanalysis data revealed a robust agreement in most patterns, while also highlighting areas where reanalysis data could complement observational gaps. This approach was critical in ensuring the reliability of our findings and in understanding the limitations and strengths of different data sources.

In Stage 2, the most important scientific investigations of the project were performed. Advanced statistical techniques we employed to link total cloud cover (TCC), sea ice concentration (SIC), and sea surface temperatures (SST), uncovering global coupled patterns and their physical mechanisms.

Stage 3 | Anthropogenic and natural footprints identified using cloud cover and sea ice outputs from the Alfred Wegener Institute Earth System Model (AWI-ESM)

The Alfred Wegener Institute Earth System Model (AWI-ESM, version 2.1) is a state-of-the-art coupled climate model that includes dynamics of land carbon cycle and vegetation. The AWI-ESM2.1 comprises the atmospheric component ECHAM6, that is based on a spectral dynamical core and includes the land surface and carbon cycle model JSBACH, as well as the Finite Volume Sea-Ice–Ocean Model FESOM2 that simulates ocean and sea-ice dynamics (Sidorenko et al. 2019). The JSBACH simulates the land-based part of the carbon cycle and vegetation dynamics. Earth ‘s complex natural vegetation is simplified in the model via plant functional types that may dynamically adjust to, and feedback on, changes in ambient climate. The FESOM2 is based on the finite volume approach formulated on unstructured meshes. This numerical method facilitates a very flexible representation of spatial resolution and enables representation of spatially small-scale processes in the global domain while limiting numerical expense. The spatially varying resolution reaches down to 15 km across polar and coastal regions and is in the range of 135 km for the far-field ocean (Sidorenko et al. 2019). The link from local dynamics on the global ocean in FESOM2’s multi-resolution approach has been verified in a number of FESOM-based studies (Vaideanu et al. 2023b). In this project we focus our analysis on spatially resolved SST and SIC interpolated from the native irregular mesh of the ocean model to a regular grid of 1°x 1° resolution.

3.1 Preform simulations with AWI-ESM2.1 model under different scenarios of increasing atmospheric CO₂ concentration

The AWI-ESM2.1 has been validated for various different climate states including the modern, the early-Holocene, the Last Interglacial, and the Last Glacial Maximum (Vaideanu et al. 2023b). All modelled quantities presented in this project refer to two CMIP6 DECK simulations: historical, that provides transient climate over the industrial era spanning the period from 1850-2014, and piControl, that provides a quasi-equilibrium preindustrial climate state spanning 250 model years. The historical simulation was initialized with the equilibrated state derived from the preindustrial simulation. Both simulations follow the CMIP6

protocol and are driven by the respective climate forcing. The piControl simulation is exposed to a constant orbital and greenhouse gas forcing that refers to unperturbed 1850 conditions. In contrast, the historical simulation is forced with observed/reconstructed concentrations of relevant greenhouse, volcanic aerosols and solar forcing. In the preindustrial state the vegetation can evolve freely in the model based on the AWI-ESM's implementation of vegetation dynamics. As the historical simulation must represent land cover changes, that occurred during the historical period, precisely in order to create a modelled climate evolution that is as comparable as possible to that derived from observations, dynamic vegetation is deactivated in this simulation and global vegetation cover is instead prescribed as a global time-varying data set (Vaideanu et al. 2023b).

3.2 Canonical Correlation Analysis (CCA) between Sea Ice Concentration (SIC) with Sea Surface Temperature (SST) fields, using AWI-ESM2.1 data

Multiple CCAs were performed on detrended annual anomalies of Atlantic SST and Arctic SIC from AWI-ESM2.1 historical simulation (1850-2014) to verify results from observed and reanalysis Arctic SIC data. The first coupled SST-SIC pair (Fig R9, left side) shows strong positive SST anomalies northeast of Greenland and negative anomalies over the subpolar gyre and much of the South Atlantic, explaining 20% of SST variance. While this pattern resembles observed SST anomalies (Fig 2a), the model produces more intense negative anomalies over the subpolar gyre, likely due to a known bias in Southern Ocean SST. The corresponding SIC pattern explains 11% of the variance and exhibits negative anomalies across most of the Arctic, aligning well with observations. The time series of these structures is moderately correlated ($r=0.46$) with the simulated Atlantic Meridional Overturning Circulation (AMOC) index.

The second SST-SIC pair (Figure R9, right side) explains 9.5% of SST variance, showing positive anomalies over the subpolar gyre, negative anomalies in the western subtropical North Atlantic, and warm anomalies between the equator and 30°N. This pattern is similar to the NAO-like SST response obtained from observations. The associated SIC pattern explains 3% of SIC variance and includes positive anomalies in the Barents and Kara Seas and negative anomalies in Baffin Bay, similar with the NAO-linked observed Arctic SIC pattern, though the explained variance is much lower.

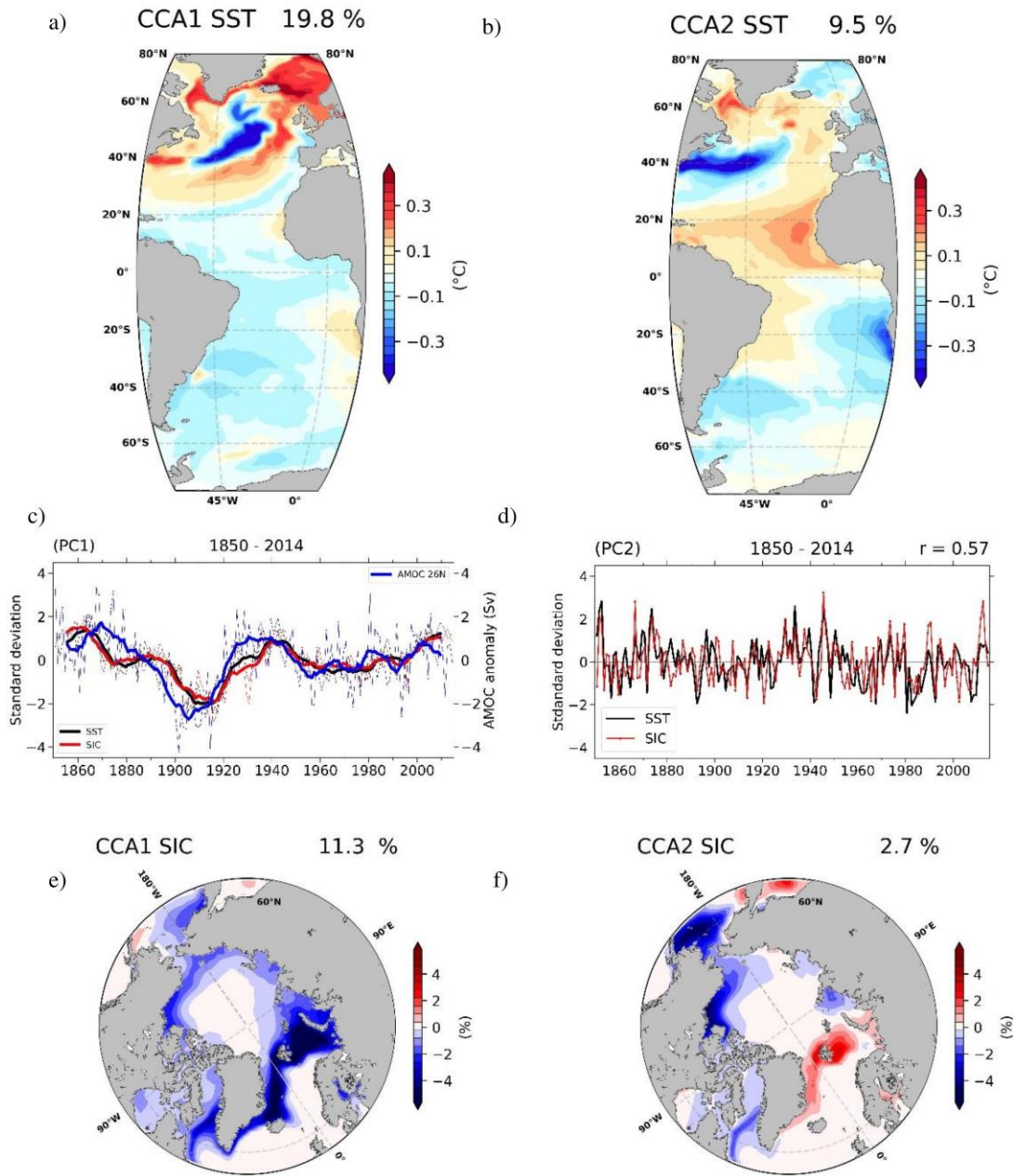


Figure R9. Simulated coupled SST-SIC patterns identified through CCA between the corresponding AWI-ESM-2.1 “historical” annual detrended anomalies from 1850–2014. *Left column:* The SST ($^{\circ}\text{C}$) pattern (a) of the first pair, explaining 22% of variance and the SIC (%) structure (e), explaining 10% of variance. Their associated time series (c) with SIC (red line), SST (black line) are plotted with an 11yr running mean and have a correlation coefficient of 0.84. Their correlation with the simulated AMOC Index, defined as the time series of annual-mean anomaly of the maximum volume transport streamfunction at 26.5°N (Sv) (blue line) is 0.48 (95% significance level). *Right column:* The SST ($^{\circ}\text{C}$) pattern of the second pair (b), explaining 14% of variance and the SIC (%) structure (f), explaining 2% of variance. Their associated time series (d), with SIC (red line), SST (black line), have a correlation coefficient of 0.65(95% significance level). **(Vaideanu et al. 2023b, Source: <https://journals.plos.org/plosone/article?id=10.1371/journal.pone.0290437>)**

The AWI-ESM2.1 model, like many CMIP6 models, exhibits a warming bias in the Antarctic/South Pole region. To reduce the impact of this bias when examining the coupled Atlantic SST-Global SIC interactions, the analysis focuses on annual SST/SIC anomalies from a preindustrial simulation, covering 250 years, with the last 100 years analyzed. The SST field of the first coupled pair (Figure R9a) explains 17% of Atlantic SST variance and shows positive anomalies along Greenland, consistent with ERA5 reanalysis (Figure R7a). However, the model reveals negative anomalies over most of the mid-latitude Atlantic, which contrasts with observed data, where a pronounced Atlantic SST dipole is evident. The associated global SIC pattern explains around 25% of the total variance, and the Arctic SIC structure (Fig 7b) aligns with the ERA5 reanalysis (Figure R7b), except for discrepancies in the Greenland, Laptev, and East-Siberian Seas, where the model shows opposite loadings. In the Southern Hemisphere (Figure R9d), the simulated SIC pattern shows positive anomalies around the Antarctic Peninsula and the Indian Ocean sector of the Southern Ocean, similar to ERA5 reanalysis results. However, significant negative anomalies are present over the Weddell and Ross Seas, differing from ERA5 SIC data. This discrepancy may be related to the model's persistent SST bias, which impacts sea ice formation by suppressing it. The temporal evolution of the SST-SIC spatial patterns is moderately correlated ($r=0.37$) with the AMOC index from the simulation, suggesting a link between modeled sea ice and ocean circulation variability.

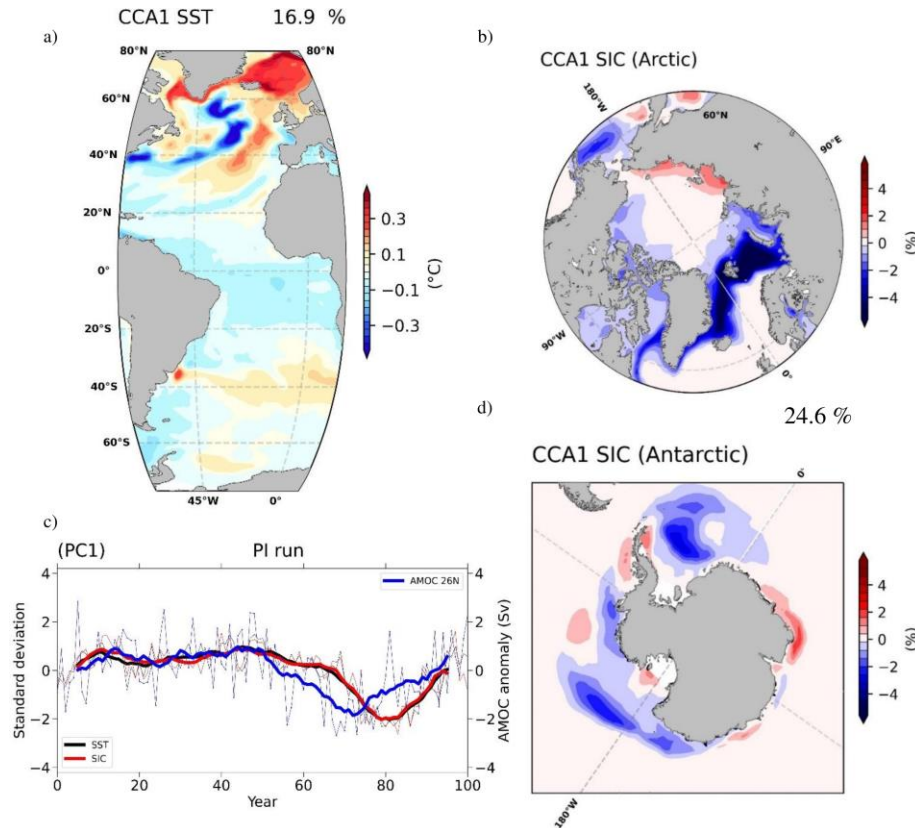


Figure R10. Simulated coupled Atlantic SST - Global SIC patterns identified through CCA between the corresponding AWIESM2.1 PI annual anomalies extending over 100 years. Pattern of SST ($^{\circ}\text{C}$) (a) and of the Arctic (b) and Antarctic (d) SIC (%) from the first coupled CCA pair. Their associated time

series (c) with SIC (red line), SST (black line) are plotted with an 11yr running mean and have a correlation with the simulated AMOC Index, defined as the time series of annual-mean anomaly of the maximum volume transport streamfunction at 26.5°N (Sv) (blue line) of 0.37 (95% significance level).

In Stage 3 the analysis of SST and SIC anomalies from AWI-ESM2.1 provide valuable insights into the coupled variability between these two climate components under different atmospheric CO₂ concentrations. Despite model biases, the model reproduces key aspects of the observed SST and SIC spatial structures, particularly in the Northern Hemisphere. Overall, this stage underscores the importance of understanding both anthropogenic and natural induced impact in interpreting long-term sea ice and ocean temperature changes.

The project successfully met its goals, advancing understanding of anthropogenic and natural induced climate variability and contributing to reducing uncertainty in climate models. Results were disseminated through five scientific papers, three of which are already published, and two are currently under review. The project also fostered important international collaborations, notably with the Alfred Wegener Institute, and has implications for both climate science and policymaking.

Dr. Petru-Cosmin Vaideanu



IPCC, Masson-Delmotte V, Zhai P, et al (2021) Climate Change 2021: The Physical Science Basis. Contribution of Working Group I to the Sixth Assessment Report of the Intergovernmental Panel on Climate Change

Jackson LC, Kahana R, Graham T, et al (2015) Global and European climate impacts of a slowdown of the AMOC in a high resolution GCM. *Clim Dyn* 45:. <https://doi.org/10.1007/s00382-015-2540-2>

Levine RA, Wilks DS (2000) Statistical Methods in the Atmospheric Sciences. *J Am Stat Assoc.* <https://doi.org/10.2307/2669579>

Lorenz EN (1951) SEASONAL AND IRREGULAR VARIATIONS OF THE NORTHERN HEMISPHERE SEA-LEVEL PRESSURE PROFILE. *Journal of Meteorology.* [https://doi.org/10.1175/1520-0469\(1951\)008<0052:saivot>2.0.co;2](https://doi.org/10.1175/1520-0469(1951)008<0052:saivot>2.0.co;2)

Norris JR, Allen RJ, Evan AT, et al (2016) Evidence for climate change in the satellite cloud record. *Nature.* <https://doi.org/10.1038/nature18273>

Sidorenko D, Goessling HF, Koldunov N V., et al (2019) Evaluation of FESOM2.0 Coupled to ECHAM6.3: Preindustrial and HighResMIP Simulations. *J Adv Model Earth Syst* 11:. <https://doi.org/10.1029/2019MS001696>

Vaideanu P, Ionita M, Voiculescu M, Rimbu N (2023a) Deconstructing Global Observed and Reanalysis Total Cloud Cover Fields Based on Pacific Climate Modes. *Atmosphere (Basel)* 14:. <https://doi.org/10.3390/atmos14030456>

Vaideanu P, Stepanek C, Dima M, et al (2023b) Large-scale sea ice-Surface temperature variability linked to Atlantic meridional overturning circulation. *PLoS One* 18:. <https://doi.org/10.1371/journal.pone.0290437>